RESEARCH ARTICLE
SPACE PHYSICS: IONOSPHERIC PHYSICS

Earth and Planetary Physics
10: 447–453, 2026
doi: 10.26464/epp2026048

Rocket-induced lower ionosphere disturbances derived from measurements of very low frequency transmitter signals

JingYuan Feng[1], Wei Xu[1,2*], XuDong Gu[1,2,3], BinBin Ni[1,2], ShiWei Wang[1], Bin Li[3,4*], Ze-Jun Hu[3,4], Fang He[3], Xiang-Cai Chen[3,4], and Hong-Qiao Hu[3]

[1]School of Earth and Space Science and Technology, Wuhan University, Wuhan 430072, China;

[2]Hubei Luojia Laboratory, Wuhan 430072, China;

[3]Antarctic Zhongshan Ice and Space Environment National Observation and Research Station, Polar Research Institute of China, Shanghai 200136, China;

[4]Center for Space Physics and Astronomy, Polar Research Institute of China, Shanghai 200136, China

Key Points:

- We report wavelike perturbations in measurements of very low frequency (VLF) transmitter signals triggered by a rocket launch event in North America.
- The perturbations caused by the rocket launch event exhibit a common feature of two isolated pulses with a period of 3.5–7 min.
- The two-pulse perturbations measured in VLF signals are likely caused by shock acoustic waves and the surface reflection.

Citation: Feng, J. Y., Xu, W., Gu, X. D., Ni, B. B., Wang, S. W., Li, B., Hu, Z.-J., He, F., Chen, X.-C., and Hu, H.-Q. (2026). Rocket-induced lower ionosphere disturbances derived from measurements of very low frequency transmitter signals. *Earth Planet. Phys.*, *10*(3), 447–453. http://doi.org/10.26464/epp2026048

Abstract: A rocket launch can induce large-scale atmospheric disturbances, which have mainly been investigated in previous studies by using measurements of total electron content. In this study, we report the perturbation in very low frequency (VLF) transmitter signals triggered by a rocket launch event, which, unlike total electron content measurements, is directly related to the *D*-region ionosphere. The perturbation in VLF measurements typically occurred ~9 min after liftoff, resulting in an amplitude change of up to 2.82 dB, and it had a common period of ~3.5–7 min. Moreover, the perturbation consisted of two isolated pulses, a feature notably different from previous measurements. Given the close correlation between the rocket launch and the VLF measurements, as well as the similarity between different propagation paths, these perturbations were likely caused by shock acoustic waves generated during the rocket launch because the periods were similar.

Keywords: *D*-region ionosphere; rocket launch; subionospheric VLF technique; VLF remote sensing; atmospheric waves; atmospheric disturbance

1. Introduction

The *D*-region ionosphere (60–100 km), as a part of the mesosphere and lower thermosphere region, is a critical layer of the Earth's atmosphere (Wait and Spies, 1964; McRae and Thomson, 2004). As the upper boundary of the Earth–ionosphere waveguide, the *D*-region ionosphere controls the propagation of radio waves in the very low frequency (VLF) range (3–30 kHz), which can travel for long distances with minimal attenuation (3–4 dB/Mm; Wait and Spies, 1964). The electron density of the *D*-region ionosphere is highly variant (Thomson et al., 2007) as it is influenced by various space weather events (Inan et al., 2010). Measurements of VLF transmitter signals have been utilized to investigate the *D*-region ionosphere during solar flares (McRae and Thomson, 2004; Xu W et al., 2023b), solar eclipses (Singh et al., 2011; Chakraborty et al., 2016; Xu W et al., 2019), and energetic particle precipitation from the Van Allen radiation belts (Rodger et al., 2007; Clilverd et al., 2020), as well as gamma-ray bursts (Fishman and Inan, 1988; Cheng et al., 2024). However, because of the challenges of directly observing this altitude range, this region remains one of the least explored in the Earth's atmosphere (Clilverd et al., 2009; Inan et al., 2010). The subionospheric VLF technique remains one of the most reliable methods for investigating the variation and evolution of the *D*-region ionosphere (Cummer et al., 1998; Thomson, 2010).

In addition to the above-mentioned events, the *D*-region is influenced by atmospheric waves propagating upward from the lower atmosphere (Haldoupis and Pancheva, 2002; Haldoupis et al., 2004; Silber and Price, 2017). Gravity waves (GWs) and shock acoustic waves (SAWs) are two important wave types that are often generated by natural events, such as volcanic eruptions, earthquakes, and thunderstorm activity (NaitAmor et al., 2018; Mahmoudian et al., 2021). Besides natural sources, human activity

First author: J. Y. Feng, jingyuanf@whu.edu.cn
Correspondence to: W. Xu, wei.xu@whu.edu.cn
B. Li, libin@pric.org.cn
Received 06 NOV 2025; Accepted 07 APR 2026.
First Published online 30 APR 2026.

can drive large-scale atmospheric disturbances; rocket launches are well known to be capable of generating impulsive atmospheric SAWs and GWs (Lin CCH et al., 2017a, 2017b; Chou MY et al., 2018). To analyze the impacts of rocket launches on the ionosphere, various studies have utilized measurements of the total electron content (TEC). Mendillo et al. (1975) first reported TEC depletion following the launch of the Skylab space station, whereas Lin CCH et al. (2017a) observed concentric traveling ionospheric disturbances that were consistent with the dispersion relation of GWs. Moreover, Chou MY et al. (2018) revealed that gigantic SAWs were generated during the launch of the SpaceX Falcon 9 rocket. More recently, Park et al. (2022) found plasma density holes lasting for several hours after a Falcon rocket launch near Cape Canaveral. However, these studies were mostly based on TEC measurements, which are more closely related to the *F*-region electron density. How the *D*-region, through which the atmospheric disturbance would propagate, is influenced by rocket launches has rarely been investigated.

Measurements of VLF transmitter signals are particularly suitable for resolving this problem because they carry direct information about the *D*-region ionosphere (McRae and Thomson, 2004). Compared with TEC measurements, the VLF technique can capture rapid and localized disturbances in the lower ionosphere with high sensitivity and wide spatial coverage (Marshall and Snively, 2014; Yue J and Lyons, 2015). It has therefore been widely used to analyze the ionospheric disturbances caused by cyclones, thunderstorms, and semidiurnal tides (NaitAmor et al., 2018; Patil et al., 2024). NaitAmor et al. (2018) reported measurements of the wavelike feature from VLF transmitter signals, which was suggested to originate from traveling ionospheric disturbances (TIDs) resulting from GWs generated by tropical storms and hurricanes. Mahmoudian et al. (2021) found that VLF measurements could be utilized to investigate the evolution of the semidiurnal tides in various regions with high spatial resolution. Patil et al. (2024) analyzed VLF measurements during the cyclonic storm Fani and found oscillations with periods of 13–20 min from the VLF measurements. Nevertheless, measurements of the VLF disturbance caused by rocket launches have not been reported previously. Saha et al. (2020) reported the VLF disturbance induced by the launch of the Geosynchronous Satellite Launch Vehicle rocket from Sriharikota, India, on August 27, 2015. The disturbance occurred 134 s after the rocket launch, and the amplitude change was ~3 dB.

In this study, we report the wavelike perturbations of VLF transmitter signals induced by rocket launches event in North America. These VLF perturbations were different from those reported by Saha et al. (2020) and consisted of two isolated pulses with a common period of 3.5–7 min. We quantified the periodic oscillation, spatial variations, and how they related to rocket-induced atmospheric waves. This study provides new insights into how rocket launches influence the lower ionosphere and demonstrates the capability of VLF measurements as an effective tool to monitor atmospheric disturbance.

2. Instrument and Data

The data utilized in this study were recorded using the VLF wave detection system developed by Wuhan University (Zhou RX et al., 2020; Gu XD et al., 2022b). This system can detect radio waves with frequencies between 1 and 50 kHz, with a dynamic range of ~110 dB and a timing accuracy of ~100 ns. Its core components include magnetic loop antennas, an analog front end, and a digital receiver module (Gu XD et al., 2022b). Similar to the Atmospheric Weather Electromagnetic System for Observation, Modeling, and Education (AWESOME) instrument (Cohen et al., 2010), two triangle-shaped magnetic loop antennas were set up orthogonally in the east–west and north–south directions. We established a network consisting of 10 receivers in the central area of China, as well as another receiver at the Great Wall Station (GWS) in Antarctica. The VLF data collected from this network have been widely used in studies of ionospheric and atmospheric phenomena, such as lightning discharges (Yi J et al., 2020; Gu XD et al., 2021; Xu W et al., 2023a), solar flares (Gu XD et al., 2023; Wang SW et al., 2024), solar eclipses (Gu XD et al., 2022a; Cheng W et al., 2023), and sunrise and sunset effects (Wang SW et al., 2020). The amplitude and phase of VLF measurements were calculated by considering that the transmitter signals were modulated by the minimum-shift keying (MSK) method. We used the amplitude data for analysis of the rocket launch in this study because the phase data are well known to be unstable (Thomson et al., 1993; Thomson et al., 2007; Gross et al., 2018). In this study, we used the VLF data collected from the GWS in Antarctica, and we mainly focused on the VLF signals transmitted from the NLK (24.8 kHz, 48.20°N, 121.92°W, Jim Creek, Washington, USA) and NML (25.2 kHz, 46.36°N, 98.34°W, LaMoure, North Dakota, USA) stations.

3. Observational Results

At 13:57:00 universal time (UT) on August 4, 2022, a New Shepard rocket was launched from the Corn Ranch Spaceport (known as Launch Site One [LSO]) near Van Horn, Texas. This rocket was a single-stage vehicle and was specifically developed for scientific experiments and space tourism. It was powered by a BE-3PM engine that utilizes liquid oxygen and hydrogen as the fuel, with a takeoff weight of ~40 tons and a payload capacity of 5 tons. According to the mission data (available at https://www.blueorigin.com), this rocket experienced the maximum dynamic pressure approximately 1 min after launch. The engine cutoff occurred at an altitude of ~57 km, approximately 2 min 21 s after liftoff, followed by the separation of the crew capsule and booster. The capsule reached its peak altitude of ~107 km approximately 1 min 42 s later. Around 5 min 35 s after the rocket launch, both the booster and the capsule began descending, eventually landing on the designated pads. The total duration from liftoff to touchdown was approximately 10 min 20 s.

We first checked the solar and geomagnetic activity before and after the rocket launch. Figure 1 presents the X-ray flux, solar wind velocity, and geomagnetic indices (disturbance storm time [*Dst*] and planetary magnetic activity [*Ap*]) from 12:00 to 24:00 UT on August 4, 2022. The X-ray fluxes remained at a low level ($<10^{-6}$ W/m^2), indicating no significant flaring activity. The solar wind velocity fluctuated around 430 km/s, whereas the *Dst* and *Ap* indices were within the ranges of 2–4 nT and 4–5 nT, respectively. The shaded region in Figure 1 marks the one-hour period following

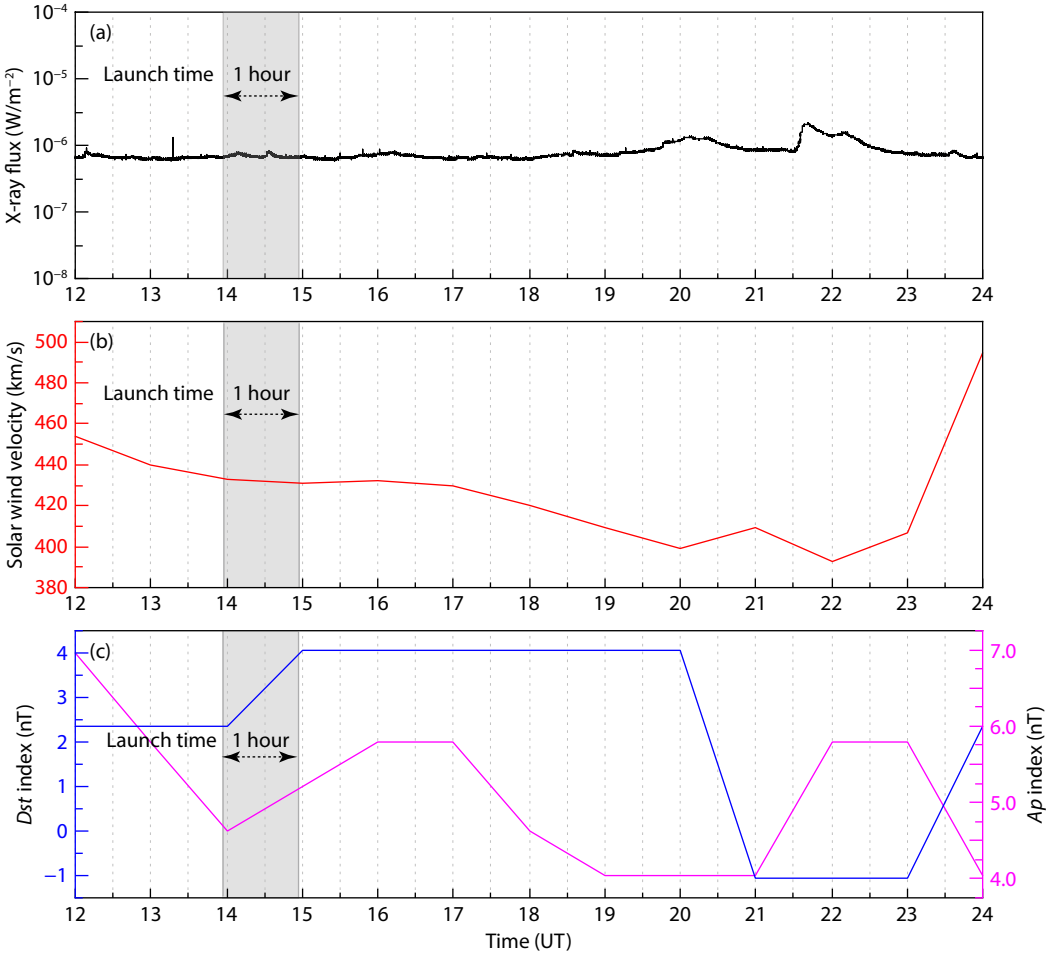

Figure 1. Solar and geomagnetic conditions from 12:00 to 24:00 UT on August 4, 2022, including the (a) X-ray flux, (b) solar wind velocity, and (c) *Dst* and *Ap* indices. The shaded region indicates the one-hour period following the rocket launch.

the launch, during which all indicators confirmed quiet solar and geomagnetic conditions. These stable conditions minimized the likelihood of space weather interference in the VLF signal observations, reinforcing the attribution of observed perturbations to the rocket launch.

Figure 2 shows the great circle paths from the NLK and NML transmitters—both of which are relatively close to LSO—to the GWS. Figures 3a and 3b show the amplitude of VLF signals emitted by the NLK and NML transmitters as received at the GWS during the rocket launch, corresponding to the NLK-GWS and NML-GWS paths, respectively. A significant increase in VLF amplitude was observed at almost the same moment from both paths, which are close to the launch site.

We first used a third-order polynomial fit to estimate the quiet-time trend for the VLF data collected before and after the event. The VLF signals exhibited typical diurnal variation caused by variation in the *D*-region ionosphere, and this step was conducted to isolate the disturbance caused solely by the rocket launch. The residual disturbances, obtained by subtracting the quiet-time trend from the raw VLF measurements, are shown in Figures 3c and 3d. For both the NLK-GWS and NML-GWS paths, the disturbance appeared to consist of two distinct phases, although the

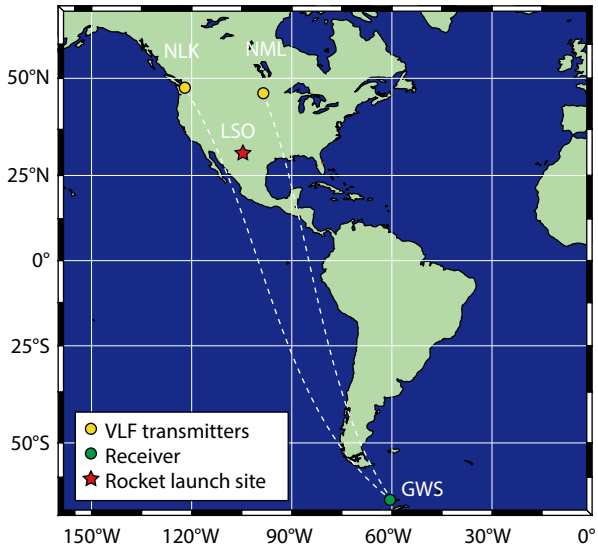

Figure 2. Great circle paths from the NLK and NML transmitters to our VLF receiver at the GWS in Antarctica. The Corn Ranch Spaceport launch site (Launch Site One [LSO]) is marked with a red star. The VLF data were collected during the rocket launch on August 4, 2022, from the NLK-GWS and NML-GWS paths.

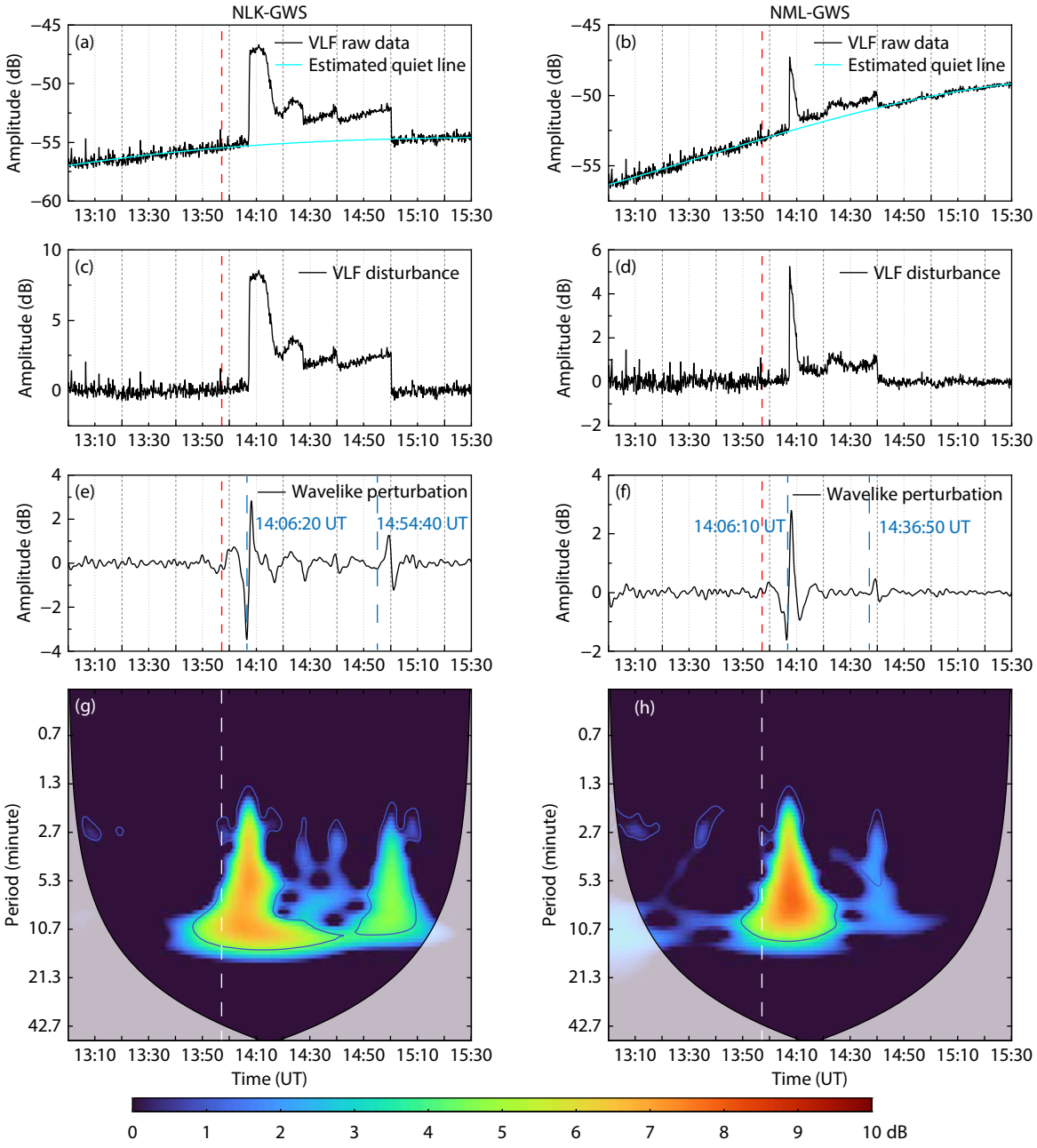

Figure 3. (a, b) The VLF raw data (black line) and estimated quiet-time curve (cyan line). (c, d) The detrended VLF disturbances. (e, f) The wavelike perturbations. (g, h) Wavelet spectra of the isolated wavelike perturbations. The black curve marks the cone of influence and the blue contours mark the 95% confidence level. The red and white dashed lines mark the rocket launch time. The blue dashed line marks the start time of the wavelike perturbations.

detailed structure was slightly different.

To extract the short-term periodic perturbation hiding in the amplitude changes, we utilized a fifth-order Butterworth bandpass filter with zero-phase forward and reverse filtering (filtfilt). The cutoff periods were set to be between 2 and 12 min, which were chosen based on previous studies on rocket-induced ionospheric disturbances (e.g., Lin CCH et al., 2017a; Liu HT et al., 2018). The filtered VLF data are shown in Figures 3e and 3f for the NLK-GWS and NML-GWS paths, respectively. For the NLK-GWS path, the wavelike perturbations comprised a large-amplitude perturbation (~2.82 dB), followed by a subsequent amplitude change of ~1.26 dB. The initial wave reached its peak at ~14:08:00 UT, and the second wave reached the maximum at ~14:59:10 UT. As for the NML-GWS path, the first amplitude change was ~2.80 dB and the second was ~0.46 dB. The corresponding times of the first and second peaks were ~14:07:50 and ~14:39:00 UT, respectively. Despite the difference in peak times, the overall structure was similar to those measured from the NLK-GWS path.

Figures 3g and 3h show the wavelet spectra of these perturbations. The black contour marks the cone of influence, and the blue

contour marks the 95% confidence level. For the NLK-GWS path, the perturbation had typical periods of ~7 and ~5.5 min. As for the NML-GWS path, the periodicity of perturbation was similar (~7 and ~3.5 min). For both paths, the periodicity was close to previously reported values for SAWs induced by rocket launches (e.g., Chou MY et al., 2018; Xie HY et al., 2025).

In addition to the periodicity, the propagation velocity is a key parameter for wave study. We estimated the horizontal velocity by using the difference in distance from the launch site to the propagation paths, as well as the time difference in the onset time of the disturbance. For example, the minimum distances were ~598 km for the NLK-GWS path and ~1101 km for the NML-GWS path, respectively, with a difference in distance of ~503 km. On the other hand, the onset time difference for these two paths was approximately 17 min 50 s (the onset time was ~14:36:50 UT for the NLK-GWS path and ~14:54:40 UT for the NML-GWS path). Therefore, the estimated propagation velocity was ~470 m/s, which is close to the typical range of SAWs triggered by rocket launches (500–1000 m/s).

4. Discussion and Conclusion

In this study, we reported the VLF disturbances caused by the rocket launch event on August 4, 2022. The VLF disturbances during the event are shown in Figure 3 and summarized in Table 1. Table 1 shows the launch site, VLF propagation paths, distances, start times, interval between the two perturbations, and periods of VLF disturbance. Note that the distance here represents the length of the great circle path between the VLF transmitter and the receiver as shown in Figure 2.

The perturbations of VLF signals typically appeared ~9 min after rocket liftoff and exhibited a clear two-stage structure. Because similar disturbances were found from the different paths for the same event, these perturbations are believed to be related more to the rocket launch than to a temporary shutdown or sudden fault of the VLF transmitters. These two-stage perturbations suggest a recurring interaction between rocket-induced atmospheric waves and the *D*-region ionosphere. This pattern is, in general, in line with previous studies: rocket launches have been found to generate TIDs and localized ionospheric anomalies (Li YQ et al., 1994; Bowling et al., 2013; Ding F et al., 2014). However, we should emphasize that the VLF disturbance reported in this study consisted of two isolated pulses, which are inherently different in form and structure from the single-peak pulse reported by Saha et al. (2020).

Moreover, the perturbations were found to have a common period of 3.5–7 min, and the speed of these disturbances, if generated by the rocket launch, was approximately 470 m/s, both of which are consistent with those of SAWs triggered by rocket launches (e.g., Lin CCH et al., 2017a; Chou MY et al., 2018; Xie HY et al., 2025). For example, Lin CCH et al. (2017a) found that the V-shaped shock acoustic wave triggered by the launch of the SpaceX Falcon 9 rocket had a period of ~8–9 min. Xie HY et al. (2025) reported a huge ionospheric hole and TIDs during a rocket launch in China; the corresponding period of ionospheric disturbances was ~7–8 min.

The two-stage perturbation in VLF measurements likely stems from complex interactions between the rocket-induced SAWs and the *D*-region ionosphere. The differences in onset time of the first and second pulses between the two propagation paths were ~10 s and ~17 min 50 s, respectively. The disturbance appeared earlier from the NML-GWS path, which is further from the launch site than the NLK-GWS path, indicating that the perturbation could not be interpreted as a simple radial horizontal propagation from the launch site. Instead, the observed timing differences more likely reflect the combined effects of vertical propagation to the altitudes of the ionosphere, horizontal expansion of the wavefront, and the path-integrated sensitivity of VLF measurements. The similarity in the periodicity and two-stage wavelike structures observed from the two paths are strongly suggestive of a wavelike disturbance associated with the rocket launch. In this study, the interval between the two perturbations was found to be ~30–48 min, which is relatively short and not likely to have been caused by long-term effects, such as the propagation of GWs (Chou MY et al., 2018). Similar phenomena of multistage ionospheric perturbations have been reported during other rocket launches. Arendt (1971) first reported a multiple-stage perturbation induced by the launch of Apollo 14, and the separation time between the different stages was approximately 1 h. The perturbation mainly occurred at the bottom of the *F*-region and was suggested to originate from acoustic waves triggered by the supersonic shock. Li YQ et al. (1994) reported a first pulse and a delayed wave, with an interval of ~12 min, during a space shuttle launch from Cape Canaveral and attributed the delayed wave to the surface reflection of the shuttle-generated disturbance.

Note that the VLF amplitude change during the second perturbation was smaller than that of the first perturbation, which could be due to the surface reflection, as suggested by Li YQ et al. (1994) and Lin CH et al. (2014). This speculation is also consistent with the fact that the New Shepard rocket was a single-stage launch vehicle. Furthermore, the propulsion system can contribute to a VLF disturbance. The New Shepard rocket used a hydrogen–oxygen engine, which primarily released H_2O. Previous studies have shown that these exhaust products can interact with the O^+ ions in the upper atmosphere, leading to differences in electron depletion (Mendillo et al., 1975; Bernhardt, 1987; Zhao LX et al., 2024). Similar effects could be found for the *D*-region ionosphere and need to be further investigated in future studies.

Table 1. The launch site, VLF propagation paths, distances, start times, interval between the two pulses, amplitude changes, and periods of VLF disturbance for the rocket launch event on August 4, 2022.

Launch site	Path	Distance (km)	Start time (UT)	ΔTime (min)	ΔAmplitude (dB)	Periods (min)
LSO	NLK-GWS	~929.6	~ 14:06:20 & ~14:54:40	48.33	~2.82 & ~1.26	~7 & ~5.5
	NML-GWS	~1138.5	~ 14:06:10 & ~14:36:50	30.67	~2.80 & ~0.46	~7 & ~3.5

Considering the close temporal and spatial correlation between the VLF measurements and the rocket launch, as well as the similarity between the different propagation paths, the perturbations were most likely caused by SAWs generated during the rocket launch. We have carefully checked different sources of TEC data and could find no high temporal resolution data for a more detailed analysis of these events. Future studies could use multi-instrument measurements to better understand the two-stage perturbation caused by the rocket launch. Moreover, numerical models could be utilized to verify the specific reason for the two-pulse feature. However, modeling this process and its influence on VLF signals is very complicated and requires the combination of atmospheric dynamics and chemistry models and the VLF propagation model, which we have left as the next step for a future study. The present study demonstrates the capability of the VLF technique in remotely sensing the atmospheric disturbance caused by a rocket launch, and it highlights the need for network observation of VLF signals, which could potentially infer the spatial evolution of these disturbances.

Open Research

The VLF data and codes used to generate the figures reported in this paper can be obtained from https://doi.org/10.5281/zenodo.15531305. XuDong Gu (guxudong@whu.edu.cn) is the data manager and technical engineer for the maintenance of VLF instruments and data processing.

Acknowledgments

This work was supported by the National Natural Science Foundation of China (Grant Nos. 42188101, 41874195, 42074119, 42274205, 42461160256, U2541289, U25D9004, 42130210 and 42025404), the National Key R&D Program of China (Grant No. 2022YFF0503700), the Natural Science Foundation of Hubei Province, China (Grant No. 2025AFA030), the Hubei Province Regional Science and Technology Innovation Plan Project (Grant No. 2025EHA044), and the Antarctic Zhongshan Ice and Space Environment National Observation and Research Station (Grant No. ZSNORS-20242603). The authors acknowledge the Chinese Meridian Project II, and the Chinese National Antarctic Research Expedition for support of the VLF wave detection program at the GWS and the Tencent Xplore prize.

References

Arendt, P. R. (1971). Ionospheric undulations following Apollo 14 launching. *Nature*, *231*(5303), 438–439. https://doi.org/10.1038/231438a0

Bernhardt, P. A. (1987). A critical comparison of ionospheric depletion chemicals. *J. Geophys. Res.: Space Phys.*, *92*(A5), 4617–4628. https://doi.org/10.1029/JA092iA05p04617

Bowling, T., Calais, E., and Haase, J. S. (2013). Detection and modelling of the ionospheric perturbation caused by a Space Shuttle launch using a network of ground-based Global Positioning System stations. *Geophys. J. Int.*, *192*(3), 1324–1331. https://doi.org/10.1093/gji/ggs101

Chakraborty, S., Palit, S., Ray, S., and Chakrabarti, S. K. (2016). Modeling of the lower ionospheric response and VLF signal modulation during a total solar eclipse using ionospheric chemistry and LWPC. *Astrophys. Space Sci.*, *361*(2), 72. https://doi.org/10.1007/s10509-016-2660-0

Cheng, W., Xu, W., Gu, X. D., Wang, S. W., Wang, Q. S., Ni, B. B., Lu, Z. L., Xiao, B. X., and Meng, X. Y. (2023). A comparative study of VLF transmitter signal measurements and simulations during two solar eclipse events. *Remote Sens.*, *15*(12), 3025. https://doi.org/10.3390/rs15123025

Cheng, W., Xu, W., Xiong, S. L., Gu, X. D., Ni, B. B., Wang, C. W., Zhang, Y. Q., Wang, S. W., Feng, J. Y., … Ma, W. C. (2024). Spectra of GRB 221009A at low energies derived from ground-based very low-frequency measurements. *Astrophys. J.*, *971*(1), 55. https://doi.org/10.3847/1538-4357/ad5cec

Chou, M. Y., Shen, M. H., Lin, C. C. H., Yue, J., Chen, C. H., Liu, J. Y., and Lin, J. T. (2018). Gigantic circular shock acoustic waves in the ionosphere triggered by the launch of FORMOSAT-5 satellite. *Space Weather*, *16*(2), 172–184. https://doi.org/10.1002/2017SW001738

Clilverd, M. A., Rodger, C. J., Thomson, N. R., Brundell, J. B., Ulich, T., Lichtenberger, J., Cobbett, N., Collier, A. B., Menk, F. W., … Turunen, E. (2009). Remote sensing space weather events: Antarctic-Arctic Radiation-belt (Dynamic) Deposition-VLF Atmospheric Research Konsortium network. *Space Wea.*, *7*(4), S04001. https://doi.org/10.1029/2008SW000412

Clilverd, M. A., Rodger, C. J., van de Kamp, M., and Verronen, P. T. (2020). Electron precipitation from the outer radiation belt during the St. Patrick's Day storm 2015: Observations, modeling, and validation. *J. Geophys. Res.: Space Phys.*, *125*(2), e2019JA027725. https://doi.org/10.1029/2019JA027725

Cohen, M. B., Inan, U. S., and Paschal, E. W. (2010). Sensitive broadband ELF/VLF radio reception with the AWESOME instrument. *IEEE Trans. Geosci. Remote Sens.*, *48*(1), 3–17. https://doi.org/10.1109/TGRS.2009.2028334

Cummer, S. A., Inan, U. S., and Bell, T. F. (1998). Ionospheric *D* region remote sensing using VLF radio atmospherics. *Radio Sci.*, *33*(6), 1781–1792. https://doi.org/10.1029/98RS02381

Ding, F., Wan, W. X., Mao, T., Wang, M., Ning, B. Q., Zhao, B. Q., and Xiong, B. (2014). Ionospheric response to the shock and acoustic waves excited by the launch of the Shenzhou 10 spacecraft. *Geophys. Res. Lett.*, *41*(10), 3351–3358. https://doi.org/10.1002/2014GL060107

Fishman, G. J., and Inan, U. S. (1988). Observation of an ionospheric disturbance caused by a gamma-ray burst. *Nature*, *331*(6155), 418–420. https://doi.org/10.1038/331418a0

Gross, N. C., Cohen, M. B., Said, R. K., and Gołkowski, M. (2018). Polarization of narrowband VLF transmitter signals as an ionospheric diagnostic. *J. Geophys. Res.: Space Phys.*, *123*(1), 901–917. https://doi.org/10.1002/2017JA024907

Gu, X. D., Li, G. J., Pang, H., Wang, S. W., Ni, B. B., Luo, F., Peng, R., and Chen, L. (2021). Statistical analysis of very low frequency atmospheric noise caused by the global lightning using ground-based observations in China. *J. Geophys. Res.: Space Phys.*, *126*(6), e2020JA029101. https://doi.org/10.1029/2020JA029101

Gu, X. D., Peng, R., Wang, S. W., Ni, B. B., Luo, F., Li, G. J., and Li, Z. P. (2022a). Responses of the very low frequency transmitter signals during the solar eclipse on December 26, 2019 over a north–south propagation path. *IEEE Trans. Geosci. Remote Sens.*, *60*, 2000207. https://doi.org/10.1109/TGRS.2021.3056092

Gu, X. D., Wang, Q. S., Ni, B. B., Xu, W., Wang, S. W., Yi, J., Hu, Z. J., Li, B., He, F., … Hu, H. Q. (2022b). First results of the wave measurements by the WHU VLF wave detection system at the Chinese Great Wall station in Antarctica. *J. Geophys. Res.: Space Phys.*, *127*(9), e2022JA030784. https://doi.org/10.1029/2022JA030784

Gu, X. D., Yi, J., Wang, S. W., Hu, Z. J., Xu, W., Ni, B. B., Li, B., He, F., Chen, X. C., and Hu, H. Q. (2023). Comparison of VLF signal responses to solar flares along daytime and nighttime propagation paths. *Remote Sens.*, *15*(4), 1018. https://doi.org/10.3390/rs15041018

Haldoupis, C., and Pancheva, D. (2002). Planetary waves and midlatitude sporadic *E* layers: Strong experimental evidence for a close relationship. *J. Geophys. Res.*, *107*(A6), 1078. https://doi.org/10.1029/2001JA000212

Haldoupis, C., Pancheva, D., and Mitchell, N. J. (2004). A study of tidal and planetary wave periodicities present in midlatitude sporadic *E* layers. *J. Geophys. Res.*, *109*(A2), A02302. https://doi.org/10.1029/2003JA010253

Inan, U. S., Cummer, S. A., and Marshall, R. A. (2010). A survey of ELF and VLF research on lightning-ionosphere interactions and causative discharges. *J. Geophys. Res.: Space Phys.*, *115*(A6), A00E36. https://doi.org/10.1029/

2009JA014775

Li, Y. Q., Jacobson, A. R., Carlos, R. C., Massey, R. S., Taranenko, Y. N., and Wu, G. (1994). The blast wave of the Shuttle plume at ionospheric heights. *Geophys. Res. Lett.*, *21*(24), 2737–2740. https://doi.org/10.1029/94GL02548

Lin, C. C. H., Shen, M. H., Chou, M. Y., Chen, C. H., Yue, J., Chen, P. C., and Matsumura, M. (2017a). Concentric traveling ionospheric disturbances triggered by the launch of a SpaceX Falcon 9 rocket. *Geophys. Res. Lett.*, *44*(15), 7578–7586. https://doi.org/10.1002/2017GL074192

Lin, C. C. H., Chen, C. H., Matsumura, M., Lin, J. T., and Kakinami, Y. (2017b). Observation and simulation of the ionosphere disturbance waves triggered by rocket exhausts. *J. Geophys. Res.: Space Phys.*, *122*(8), 8868–8882. https://doi.org/10.1002/2017JA023951

Lin, C. H., Lin, J. T., Chen, C. H., Liu, J. Y., Sun, Y. Y., Kakinami, Y., Matsumura, M., Chen, W. H., Liu, H., and Rau, R. J. (2014). Ionospheric shock waves triggered by rockets. *Ann. Geophys.*, *32*(9), 1145–1152. https://doi.org/10.5194/angeo-32-1145-2014

Liu, H. T., Ding, F., Yue, X. N., Zhao, B. Q., Song, Q., Wan, W. X., Ning, B. Q., and Zhang, K. K. (2018). Depletion and traveling ionospheric disturbances generated by two launches of China's Long March 4B rocket. *J. Geophys. Res.: Space Phys.*, *123*(12), 10319–10330. https://doi.org/10.1029/2018JA026096

Mahmoudian, A., Mohebalhojeh, A. R., and Safari, M. (2021). Investigation of VLF radio sounding for studying semi-diurnal tide and gravity waves. *Geophys. Res. Lett.*, *48*(8), e2021GL092949. https://doi.org/10.1029/2021GL092949

Marshall, R. A., and Snively, J. B. (2014). Very low frequency subionospheric remote sensing of thunderstorm-driven acoustic waves in the lower ionosphere. *J. Geophys. Res.: Atmos.*, *119*(9), 5037–5045. https://doi.org/10.1002/2014JD021594

McRae, W. M., and Thomson, N. R. (2004). Solar flare induced ionospheric D-region enhancements from VLF phase and amplitude observations. *J. Atmos. Sol.-Terr. Phys.*, *66*(1), 77–87. https://doi.org/10.1016/j.jastp.2003.09.009

Mendillo, M., Hawkins, G. S., and Klobuchar, J. A. (1975). A sudden vanishing of the ionospheric *F* region due to the launch of Skylab. *J. Geophys. Res.*, *80*(16), 2217–2228. https://doi.org/10.1029/JA080i016p02217

NaitAmor, S., Cohen, M. B., Kumar, S., Chanrion, O., and Neubert, T. (2018). VLF signal anomalies during cyclone activity in the Atlantic Ocean. *Geophys. Res. Lett.*, *45*(19), 10185–10192. https://doi.org/10.1029/2018GL078988

Park, J., Rajesh, P. K., Ivarsen, M. F., Lin, C. C. H., Eastes, R. W., Chao, C. K., Coster, A. J., Clausen, L., and Burchill, J. K. (2022). Coordinated observations of rocket exhaust depletion: GOLD, madrigal TEC, and multiple low-Earth-orbit satellites. *J. Geophys. Res.: Space Phys.*, *127*(2), e2021JA029909. https://doi.org/10.1029/2021JA029909

Patil, O. M., Moharana, S. S., Maurya, A. K., Parihar, N., Singh, R., and Dimri, A. P. (2024). Role of lightning activity in deciphering Atmospheric Gravity Waves (AGWs) induced D-region ionospheric perturbations during extremely severe cyclonic storm (ESCS) Fani. *J. Geophys. Res.: Space Phys.*, *129*(4), e2023JA032187. https://doi.org/10.1029/2023JA032187

Rodger, C. J., Clilverd, M. A., Nunn, D., Verronen, P. T., Bortnik, J., and Turunen, E. (2007). Storm time, short-lived bursts of relativistic electron precipitation detected by subionospheric radio wave propagation. *J. Geophys. Res.: Space Phys.*, *112*(A7), A07301. https://doi.org/10.1029/2007JA012347

Saha, K., De, B. K., Paul, B., and Guha, A. (2020). Satellite launch vehicle effect on the Earth's lower ionosphere: A case study. *Adv. Space Res.*, *65*(11), 2507–2514. https://doi.org/10.1016/j.asr.2020.02.026

Silber, I., and Price, C. (2017). On the use of VLF narrowband measurements to study the lower ionosphere and the mesosphere–lower thermosphere. *Surv. Geophys.*, *38*(2), 407–441. https://doi.org/10.1007/s10712-016-9396-9

Singh, R., Veenadhari, B., Maurya, A. K., Cohen, M. B., Kumar, S., Selvakumaran, R., Pant, P., Singh, A. K., and Inan, U. S. (2011). D-region ionosphere response to the total solar eclipse of 22 July 2009 deduced from ELF-VLF tweek observations in the Indian sector. *J. Geophys. Res.: Space Phys.*, *116*(A10), A10301. https://doi.org/10.1029/2011JA016641

Thomson, N. R. (1993). Experimental daytime VLF ionospheric parameters. *J. Atmos. Terr. Phys.*, *55*(2), 173–184. https://doi.org/10.1016/0021-9169(93)90122-F

Thomson, N. R., Clilverd, M. A., and McRae, W. M. (2007). Nighttime ionospheric *D* region parameters from VLF phase and amplitude. *J. Geophys. Res.: Space Phys.*, *112*(A7), A07304. https://doi.org/10.1029/2007JA012271

Thomson, N. R. (2010). Daytime tropical D region parameters from short path VLF phase and amplitude. *J. Geophys. Res.: Space Phys.*, *115*(A9), A09313. https://doi.org/10.1029/2010JA015355

Wait, J. R., and Spies, K. P. (1964). Characteristics of the Earth-ionosphere Waveguide for VLF Radio Waves. Washington, DC: U. S. Department of Commerce, National Bureau of Standards, 300.

Wang, S. W., Gu, X. D., Luo, F., Peng, R., Chen, H., Li, G. J., Ni, B. B., Zhao, Z. Y., and Yuan, D. (2020). Observations and analyses of the sunrise effect for NWC VLF transmitter signals. *Chin. J. Geophys. (in Chinese)*, *63*(12), 4300–4311. https://doi.org/10.6038/cjg2020O0358

Wang, S. W., Zhou, R. X., Gu, X. D., Xu, W., Hu, Z. J., Ni, B. B., Cheng, W., Feng, J. Y., Ma, W. C., … Hu, H. Q. (2024). Examining the capability of the VLF technique for nowcasting solar flares based on ground measurements in Antarctica. *Remote Sens.*, *16*(12), 2092. https://doi.org/10.3390/rs16122092

Xie, H. Y., Li, G. Z., Ding, F., Zhao, X. K., Hu, L. H., Sun, W. J., Li, Y., Li, Y., Dai, G. F., … Ning, B. Q. (2025). Traveling ionospheric disturbances with huge semicircular and circular structures triggered by two rocket launches over China. *J. Geophys. Res.: Space Phys.*, *130*(1), e2024JA033370. https://doi.org/10.1029/2024JA033370

Xu, W., Marshall, R. A., Kero, A., Turunen, E., Drob, D., Sojka, J., and Rice, D. (2019). VLF measurements and modeling of the D-region response to the 2017 total solar eclipse. *IEEE Trans. Geosci. Remote Sens.*, *57*(10), 7613–7622. https://doi.org/10.1109/TGRS.2019.2914920

Xu, W., Ma, W. C., Wang, S. W., Gu, X. D., Ni, B. B., Cheng, W., Feng, J. Y., Wang, Q. S., and Hu, M. Y. (2023a). Automatic detection of VLF tweek signals based on the YOLO model. *Remote Sens.*, *15*(20), 5019. https://doi.org/10.3390/rs15205019

Xu, W., Gu, X. D., Ni, B. B., Wang, S. W., Yang, Z., Cheng, W., Hu, Z. J., He, F., Li, B., … Hu, H. Q. (2023b). Measurements and modeling of the responses of VLF transmitter signals to X-class solar flares at the Great Wall Station in Antarctica. *Space Wea.*, *21*(4), e2022SW003249. https://doi.org/10.1029/2022SW003249

Yi, J., Gu, X. D., Cheng, W., Tang, X. Y., Chen, L., Ni, B. B., Zhou, R. X., Zhao, Z. Y., Wang, Q., and Zhou, L. Q. (2020). A detailed investigation of low latitude tweek atmospherics observed by the WHU ELF/VLF receiver: 2. Occurrence features and associated ionospheric parameters. *Earth Planet. Phys.*, *4*(3), 238–245. https://doi.org/10.26464/epp2020023

Yue, J., and Lyons, W. A. (2015). Structured elves: Modulation by convectively generated gravity waves. *Geophys. Res. Lett.*, *42*(4), 1004–1011. https://doi.org/10.1002/2014GL062612

Zhao, L. X., Ding, F., Yue, X. N., Xu, S., Wang, J. Y., Cai, Y. H., Li, M. Y., Zhang, N., Zhou, X., … Luo, J. H. (2024). Vertical structural evolution of ionospheric holes triggered by rocket launches observed by the Sanya incoherent scatter radar. *J. Geophys. Res.: Space Phys.*, *129*(12), e2024JA033171. https://doi.org/10.1029/2024JA033171

Zhou, R. X., Gu, X. D., Yang, K. X., Li, G. S., Ni, B. B., Yi, J., Chen, L., Zhao, F. T., Zhao, Z. Y., … Zhou, L. Q. (2020). A detailed investigation of low latitude tweek atmospherics observed by the WHU ELF/VLF receiver: I. Automatic detection and analysis method. *Earth Planet. Phys.*, *4*(2), 120–130. https://doi.org/10.26464/epp2020018